IEEE Access
Multidisciplinary ⋮ Rapid Review ⋮ Open Access Journal

Received 6 March 2023, accepted 18 March 2023, date of publication 27 March 2023, date of current version 30 March 2023.

Digital Object Identifier 10.1109/ACCESS.2023.3262236

RESEARCH ARTICLE

A High-Power Sandwiched Omnidirectional Circularly Polarized Antenna for GNSS Systems

MOHAMED AKMAL[1], AHMED ALIELDIN[2], (Member, IEEE), AND ANGIE R. ELDAMAK[1], (Member, IEEE)

[1]Electronics and Communications Engineering Department, Faculty of Engineering, Ain Shams University, Cairo 11566, Egypt
[2]Egyptian Technical Research and Development Centre, Cairo 11618, Egypt

Corresponding author: Mohamed Akmal (makmalmahboub@gmail.com)

ABSTRACT This paper presents a small-size, low-profile antenna for anti-attacking systems that work against unmanned GNSS-guided attacking vehicles to protect a vital area. The proposed antenna has the ability to handle, theoretically, a peak power up to 157.7 kW. It has a cylindrical shape with a diameter of 75.4 mm and a height of 12.8 mm on a low-cost FR-4 substrate. This small size allows the integration of the proposed antenna with any portable system that prevents the attacks of GNSS-guided vehicles. The proposed antenna covers the whole GNSS frequency band with a fractional impedance bandwidth of 32.5% (1.16–1.61) GHz and a fractional axial ratio bandwidth of 37.6% (1.1–1.61) GHz utilizing a sandwiched structure. This broadband performance is realized using capacitive feeding. The proposed design maintains circularly polarized radiation over a wide elevation angle of 132° and a 360° azimuth angle which makes the proposed design suitable for GNSS anti-attacking systems.

INDEX TERMS Anti-attacking, circular polarization, high power, omnidirectional, sandwiched, unmanned vehicles.

I. INTRODUCTION

Recently, the Global Navigation Satellite System (GNSS) is widely used in both civilian and military applications. The deployment of an anti-attacking system against unmanned attacking vehicles (UAVs) guided by GNSS is the most essential step used to safeguard vital targets and/or areas against these UAVs. This is achieved by primarily radiating a high-power circular-polarized (CP) wave with a wide spatial coverage around the protected area as a measure to flood the front end of the GNSS-based UAV and worsen its signal-to-noise ratio and hence lose its trajectory [1]. Therefore, many efforts have been done into designing CP antennas for such systems.

The presented antenna in [2] is CP with a low profile and an omnidirectional radiation pattern. However, it suffers from a narrow fractional impedance bandwidth (FIBW) (16.6%) and a fractional axial ratio bandwidth (FARBW) (14.8%) due to utilizing a direct coaxial feed. The authors in [3] improved the FIBW and the FARBW to 57.8% and 31% respectively at the cost of the antenna size and gain. In [4], the proposed antenna was designed to allow reconfigurable right-hand/left-hand (RH/LH) CP by utilizing PIN diodes with high gain. Unfortunately, the main drawback was its narrow FIBW (19.8%) and FARBW (25.2%). It is also worth noting that all these previously reported designs utilized Rogers RT/Duroid 5880 as a substrate which makes those designs quite costly in case of mass production. To minimize the antenna size, a few reported designs [5], [11] were implemented by adding meander-line configurations. So, a quadrature-phase difference can be executed between a part of the antenna radiating vertical linear polarization and the other part radiating horizontal polarization by meander-line configurations as in [5]. The phase difference in [6] can be implemented using a top plane with extending stubs and a bottom plane that is identical to the top plane but

The associate editor coordinating the review of this manuscript and approving it for publication was Chan Hwang See.

with a mirror. As demonstrated in [7], the phase difference is caused by the vertically suspended pins that guide vertical polarization and the horizontal parasitic strips of the antenna that guide horizontal polarization. Waveguide-based arrays feature high gain, low dielectric losses, and high-power handling capacity. In order to accomplish dual-band operation using three frequency-selective surfaces, a substrate has been integrated into a waveguide to achieve high gain (5:6 dBic) and the CP antenna, as demonstrated in [8]. The antenna in [9] is guided to be CP by loading four circular patches with different radii and L-shaped connected shorting strips onto the corners of the patch. This antenna is fed by a capacitive probe feeding to compensate the considerable probe inductance. Although a high gain is achieved, noticeable drawbacks of high cost (Taconic RF-60 substrate), large size and narrow FIBW (5.9%) and FARBW (2.44%) have been reported. The authors in [10] covered the Wi-MAX band. The design benefits from a lower Q-factor (radiation), high radiation efficiency, and higher gain because it employs a dielectric resonator antenna (DRA). It also makes use of dual L-shaped slots in the ground plane to generate orthogonal modes in a rectangular DRA excited to produce a wide CP bandwidth. In [11], a FIBW of 16.8% is achieved by a low-cost mushroom structure with four metal columns for the vertically polarized mode, while the horizontally polarized mode is achieved using a zero-phase-shift line loop. Unfortunately, the antenna has a narrow FARBW (3.13%) and low gain (0.1 dBic). The antenna in [12] supports (RH/LH) CP at the same frequency band by generating vertically polarized waves using slot loop formation and horizontally polarized waves using monopole stubs. Thus, a CP wave is created. It features high gain for both polarizations, but it suffers from very narrow FARBW and FIBW (2%). In [13], a tri-band omnidirectional CP antenna with LHCP at the first band and RHCP at the two other bands was designed based on Taconic TLY as a substrate. Unluckily, all of these bands suffer from being quite narrow indicating that the antenna can only be used in specific wireless communication systems. The proposed unidirectional antenna in [14] is based on an RHCP single substrate integrated magneto-electric dipole (MED) and is intended for lightweight wireless transceivers used in satellite communication or the sub-6 GHz band. It features high efficiency and gain but suffers from narrow FIBW (13%) and FARBW (2.5%). The presented antenna in [15] is characterized by a broad frequency band for overlapped fractional bandwidth (53.4%) and it supports CP across the entire frequency band. Unfortunately, it has several drawbacks, including having a small maximum gain (0.9 dBic), a large size ($0.4\lambda_0 \times 0.4\lambda_0 \times 0.5\lambda_0$), limited CP coverage across the elevation angle (only $\pm 5^0$) and a high cost using Rogers substrates.

To guarantee CP radiation over a large spatial coverage, the AR should maintain typically a value below 3dB over wide azimuth and elevation angles. Therefore, omnidirectional CP antennas are typically used to cover 360° in azimuth [2], [3], [4], [5], [6], [7], and [11]. However, quite a few reported designs as in [3], [4], and [6] have confirmed their small AR across elevation coverage angles of 70° in [3], 40° in [4] and 90° in [6] classifying them as the AR half power beam widths (ARHPBWs).

Concerning the power handling capability (PHC) of an antenna, many researchers have considered it as a challenging issue. So, not a few numbers of reported designs have used large metallic surfaces to improve the PHC of their antennas as in [16], [17], [18], and [19]. As a result, theoretically, a PHC of 1.16 GW is achieved in [16], 1 GW in [17], 1.29 GW in [18] and 22.9 MW in [19].

All these designs suffer from large size, heavy weight and high cost. Some other antennas that are concerned with high PHC use reflect array antennas as in [20] and [21].

In this paper, a novel CP antenna is proposed to be utilized in a GNSS anti-attacking system. The antenna has a compact size of $0.34\lambda_0 \times 0.34\lambda_0 \times 0.05\lambda_0$ (where λ_0 is the free space wavelength at the central frequency), a FIBW of 32.5% and a FARBW of 37.6%. According to [22], Fig. 1(a) is the simplest way to show that the antenna is designed to simultaneously cover the most common frequencies of the GNSS applications working across the frequency band from 1.16 to 1.61 GHz.The antenna is able to handle, theoretically, a peak power up to 157.7 kW and maintain CP radiation over a wide elevation angle of 132° and a 360° azimuth angle to ensure the maximum available spatial coverage against attackers from various directions. A possible protection scenario against UAVs using the proposed antenna is illustrated in Fig. 1(b).

II. THE PROPOSED ANTENNA

A. ANTENNA STRUCTURE

The structure of the proposed antenna is depicted in Fig. 2. The antenna consists of three stacked circular layers (layer A, layer B and layer C) arranged from top to bottom. The three layers are concentric and lie on the XY plane. Each layer is made of a low-cost FR-4 laminate with a relative permittivity $\varepsilon_r = 4.4$ and a dissipation factor of 0.025.

The three layers have thicknesses of h_1, h_2 and h_1 and radii R_p, R_2, and R_p all respectively. A copper gear-shaped patch is printed on the top side of layer A with a thickness of t. The gear-shaped patch has N poles and an inner circle of a radius R_1. Each pole has an arc-shaped edge with a length of S and every two adjacent poles are separated by a tapered slot which has a length of (R_p-R_1). A rotated replica of the gear-shaped patch is printed on the bottom side of layer C with a relative spin angle φ_N around the Z-axis. Thus, the three layers are sandwiched between the two gear-shaped patches. Each pole on layer A and its counterpart on layer C form a horizontal bowtie dipole. Therefore, the arc length S was initially designed to be $\lambda_0/4$ (where λ_0 is the free-space wavelength at the central frequency). N aluminium shorting vias are connected between the top and the bottom patches and uniformly distributed around the centre of the layers.

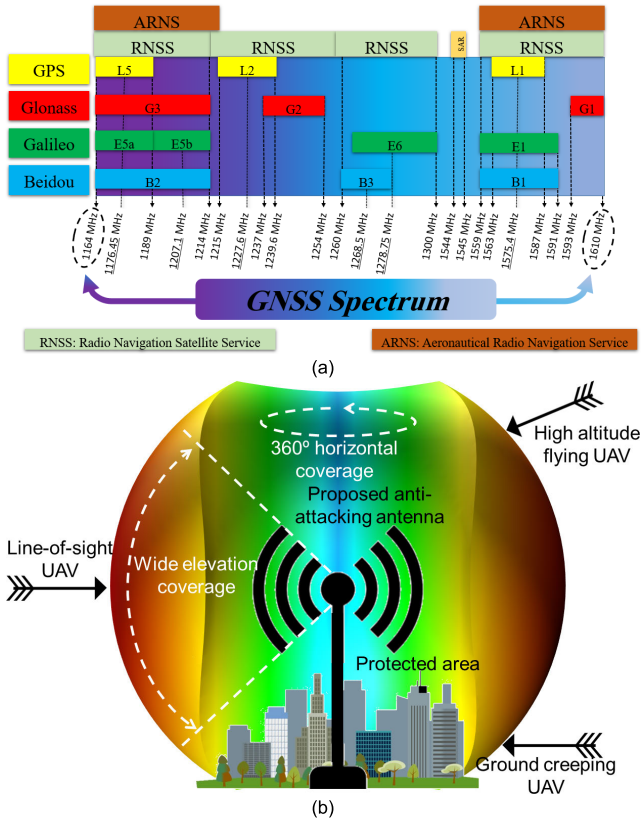

FIGURE 1. (a) GNSS frequency band; (b) Illustrative scenario of the spatial coverage provided by the proposed antenna.

TABLE 1. The optimized dimensions of the proposed antenna.

Parameters	Value	Parameters	Value
$R_p(mm)$	75.4	$r(mm)$	2.3
$R_v(mm)$	49.6	$S(mm)$	43.4
$R_1(mm)$	25	$h_1(mm)$	1.6
$R_2(mm)$	21.8	$h_2(mm)$	9.6
$R_3(mm)$	20	N	8
$t(\mu m)$	35	$\varphi_N(\text{deg})$	45

The vias are distanced by R_v from the centre of the layers and have a relative spin angle around the Z-axis of φ_N /2 with respect to both the top and the bottom patches. Each via has a cylindrical shape with a radius r. Layer B has a circular copper feeding patch on its top side with a radius of R_3.

The overall height of the antenna was initially designed to be $\lambda_g/8$ where λ_g is the guided wavelength at the central frequency and equal to $\lambda_0/\sqrt{\varepsilon_r}$. The antenna is fed through a 50Ω coaxial port attached at the centre of the layers where its inner is connected to the feeding patch on layer B while its outer is connected to the lower gear-shaped patch on layer C. It is worth noting that a small circular cut is introduced at the centre of the lower gear-shaped patch to avoid any electrical connection to the inner of the feeding port. The optimal parameters of the antenna are tabulated in TABLE 1. The antenna has been designed and simulated using Ansoft HFSS.

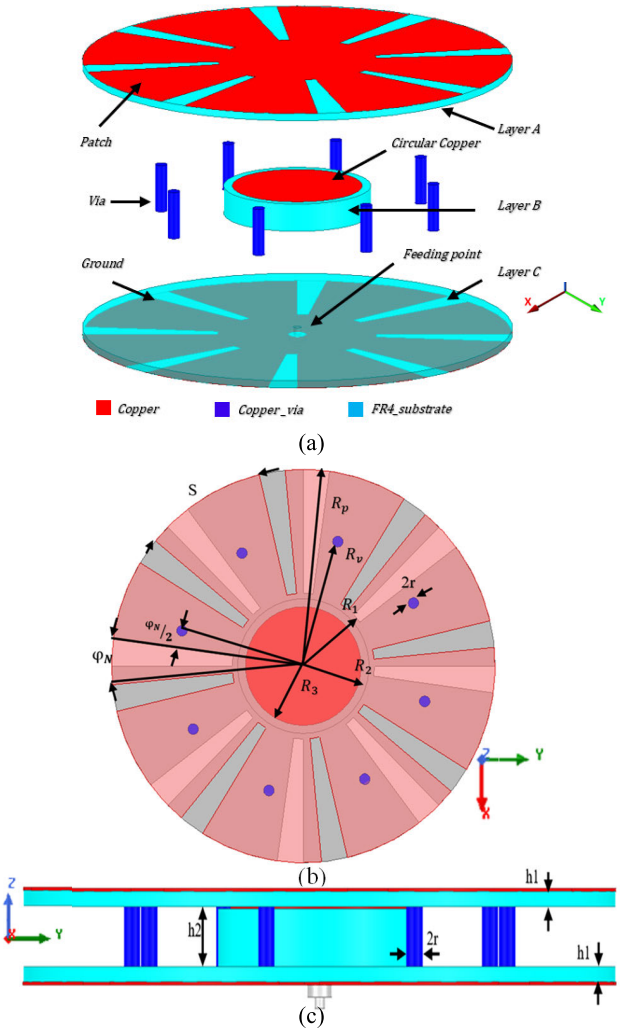

FIGURE 2. The proposed antenna: (a) Exploded structure; (b) Top view; (c) Side view.

B. ANTENNA PRINCIPLE OF OPERATION

The antenna is fed through a coaxial port where its outer is connected to the bottom gear-shaped patch and its inner is connected to the feeding patch on layer B which consequently feeds the top gear-shaped patch due to the proximity coupling across layers A. Thus, the surface current distributions across the two gear-shaped patches are of the same magnitude and in opposite directions.

The proximity coupling between the feeding patch on layer B and the top gear-shaped patch creates a capacitive loading on the antenna input impedance. However, the parallel shorting vias between the two gear-shaped patches introduce an inductive loading to the antenna input impedance. These capacitive and inductive loadings generate two relatively independent resonant frequencies across the antenna operating frequency band, the lower-resonant frequency (LRF) and the upper-resonant frequency (URF) at 1.22 GHz and 1.44 GHz, respectively as shown in Fig. 3. These two resonant frequencies are dedicated where the imaginary part of the antenna input impedance is zero. The LRF and

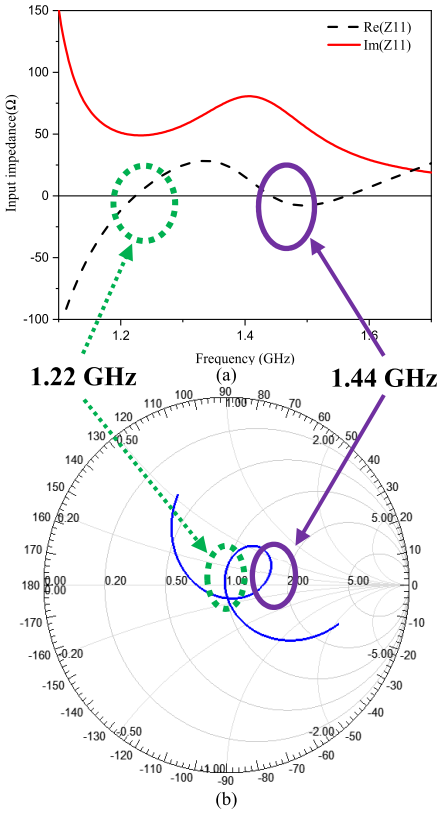

FIGURE 3. The antenna input impedance (a) *Re* and *Im* (b) Smith chart.

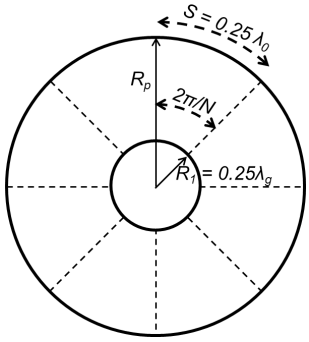

FIGURE 4. The graphical representation of the initial design.

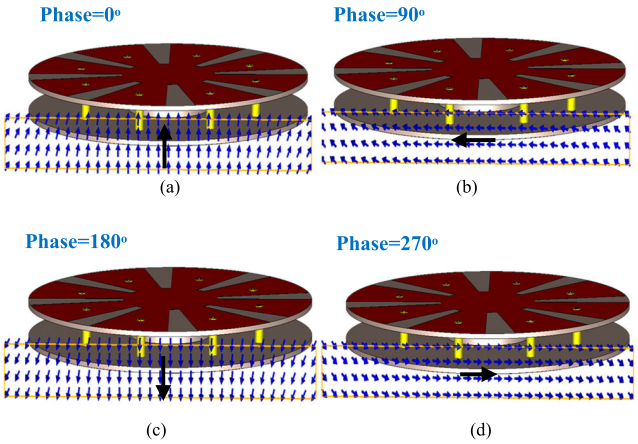

FIGURE 5. The electric field directions at (a) phase = 0°; (b) phase = 90°; (c) phase = 180°; (d) phase = 270°.

URF can be independently controlled to achieve a broad FIBW of 32.5% as going to be discussed later in the next section.

The CP is, basically, created by generating two orthogonal linearly polarized waves (vertical and horizontal) with a quad-phase shift. The vertically polarized (V-pol) wave is introduced by the two inner circles at the centre of the two gear-shaped patches while the horizontally polarized (H-pol) wave is introduced by the upper and lower poles of the two gear-shaped patches where each pair of opposite poles acts as a horizontal bowtie dipole. Therefore, at the initial phase of the design, R_1 was set to λ_g /4 such that the diameter of the inner circle ($2R_1$) equals half of the guided wavelength as shown in Fig. 4 while the arc length of each pole of the bowtie dipoles S was set to λ_0 /4. Hence, the outer radius of layers A and C can be calculated as:

$$R_p = S\frac{N}{2\pi} = \frac{N\lambda_0}{8\pi} \tag{1}$$

The length of each slot is R_p - R_1 and can be derived as:

$$R_p - R_1 = \frac{N\lambda_0}{8\pi} - \frac{\lambda_g}{4} = \lambda_0\left(\frac{N}{8\pi} - \frac{1}{4\sqrt{\varepsilon_r}}\right) \tag{2}$$

For $N = 8$ and $\varepsilon_r = 4.4$, the slot length $\approx 0.2\lambda_0$.

The quad-phase shift between the V-pol and H-pol waves is introduced by the relative spin angle between the two patches (φ_N) which is linked to the number of poles as $\varphi_N = 360/N$. So, in the proposed antenna φ_N equals 45° as a result of having 8 poles ($N = 8$). As the quad phase-shift between the V-pol and H-pol waves is an essential parameter to radiate a CP wave, the AR of the proposed antenna is sensitive to the value of φ_N as going to be discussed later in the next section. It is worth noting that the sense of rotation of the spinning angle φ_N dedicates the sense of rotation of the CP radiated waves (i.e., if φ_N = -45°, an LHCP wave will be generated).

Fig. 5 shows a section in the XZ plane of the radiated E-field at different feeding phases (0°, 90°, 180° and 270°). It can be clearly noticed from the sense of rotation of the E-filed that the antenna supports a good RHCP radiation with almost equal field strength and 90° phase rotation at the two perpendicular axes [2], and [3].

Fig. 6 shows the current distributions at 0°, 90°, 180° and 270° at the centre frequency (1.4 GHz) across the top gear-shaped patch. It is clear that the antenna has a radial current distribution at 0° and 180° while having an orthogonal tangential current distribution at 90° and 270° which guarantees good CP radiation.

III. RESULTS

A. PARAMETRIC STUDY

Number The characteristics of the proposed antenna in terms of reflection coefficient and AR will be discussed in this section. For parametric study and antenna optimization, the Ansoft High-Frequency Structure Simulator (HFSS) is

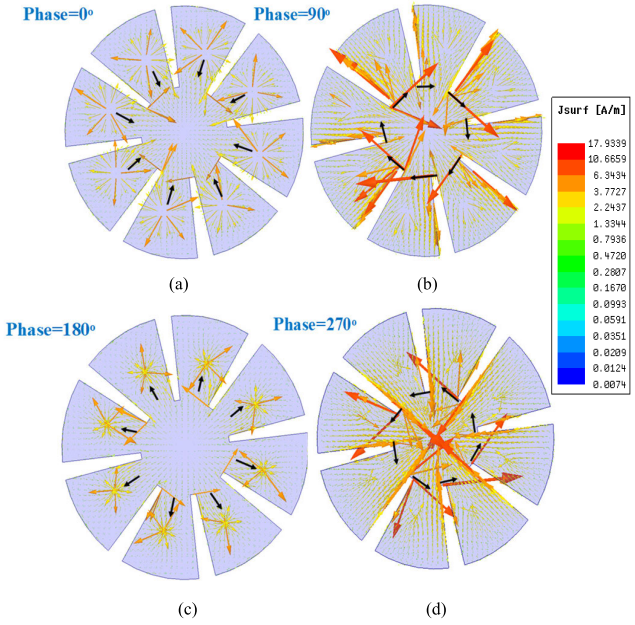

FIGURE 6. The current distributions at (a) phase = 0°; (b) phase = 90°; (c) phase = 180°; (d) phase = 270°.

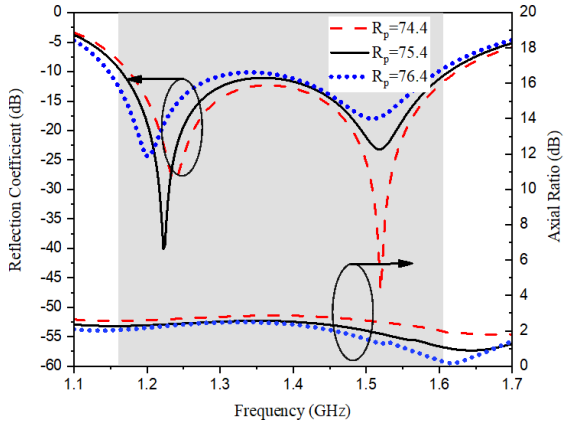

FIGURE 7. The effect of varying R_P on reflection coefficient and AR.

used. The following are the primary factors that affect the performance of the proposed antenna:

1) R_P (OUTER RADIUS OF THE ANTENNA)

The operational frequency band of the proposed design can be simply switched to another by changing the outer radius of the antenna. As shown in Fig. 7, this parameter has a considerable impact on the LRF with a slight effect on the URF. When swept upward, the frequency band is transferred to a lower band. However, changing R_P has a noticeable effect on the AR at the higher frequencies while almost no changes at the lower frequencies. The value of R_P has been optimized to be 75.4 mm.

2) R_1 (RADIUS OF THE CIRCLE OF THE GEAR-SHAPED PATCH)

This parameter has the most influence on the length of the slot and has a substantial impact on the URF. When the radius of a small patch is expanded, the URF is shifted to a lower value. From Fig. 8, when $R_1 = 49.6$ mm, the antenna works at its optimal performance with regard to covering the majority of GNSS application frequencies.

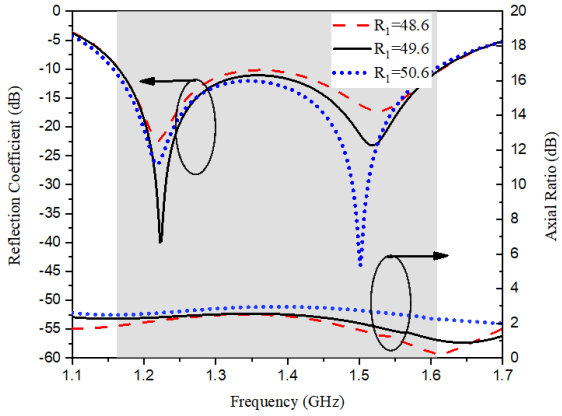

FIGURE 8. The effect of varying R_1 on reflection coefficient and AR.

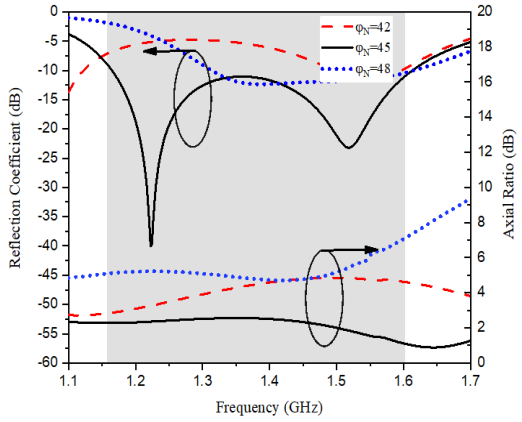

FIGURE 9. The effect of varying φ_N on reflection coefficient and AR.

3) φ_N (THE SPIN ANGLE BETWEEN THE TWO GEAR-SHAPED PATCHES)

The two orthogonal linear polarizations of the same magnitude are excited at the desired frequency band when the spin angle φ_N equals 360/N. That results in excellent broadband impedance matching and CP radiation as shown in Fig. 9. Thus, the value of spin angle φ_N is highly sensitive while constructing the CP antenna.

4) N (NUMBER OF POLES AND SHORTING-VIAS)

This parameter is studied by altering the quantity and position of the shorting vias. They act as parallel inductors. Therefore, when their number increases, their equivalent inductance decreases, and the antenna impedance goes more capacitive and vice versa as shown in the Smith chart in Fig. 10(b). When it comes to AR, the number of vias and poles is crucial. After optimizing the value of N, the proposed antenna can achieve a FARBW of 42.8% at N = 8, as shown in Fig. 10. A balance between the horizontal and vertical polarizations can be obtained by carefully tweaking the dimensional parameters.

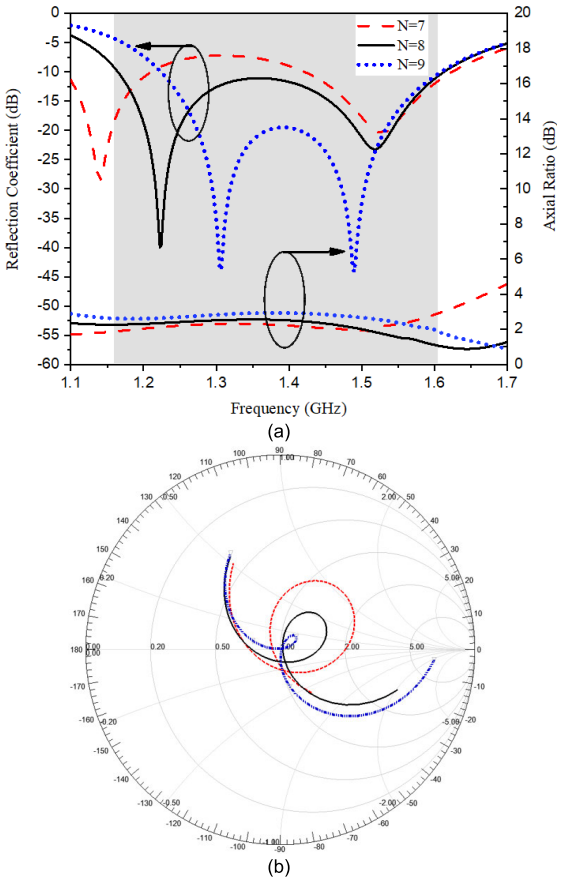

FIGURE 10. The effect of varying *N* on. (a) Reflection coefficient and AR, (b) Smith chart.

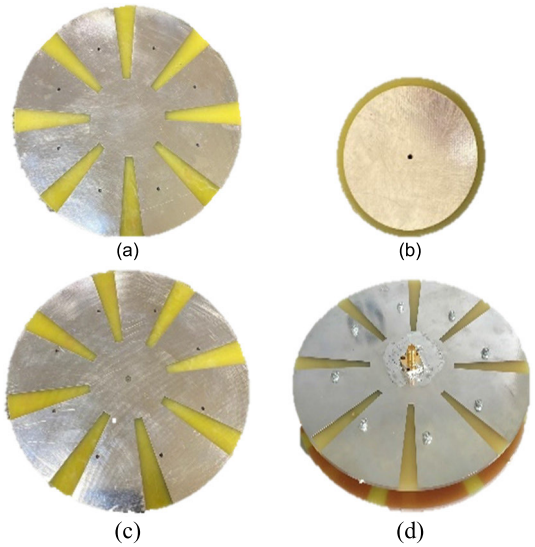

FIGURE 11. The prototype of the proposed antenna: (a) Layer A; (b) Layer B; (c) Layer C; (d) assembled structure.

B. FABRICATION AND MEASUREMENTS

To validate the idea after optimizing the antenna parameters, a prototype has been fabricated and measured. Layers A, B and C along with the assembled structure are depicted in Fig. 11. The prototype has been fabricated and assembled in

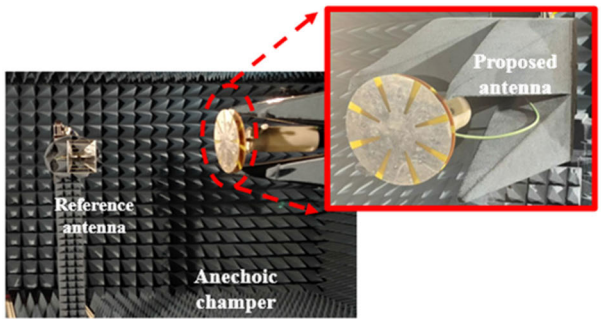

FIGURE 12. The measurement setup of the proposed antenna in an anechoic chamber.

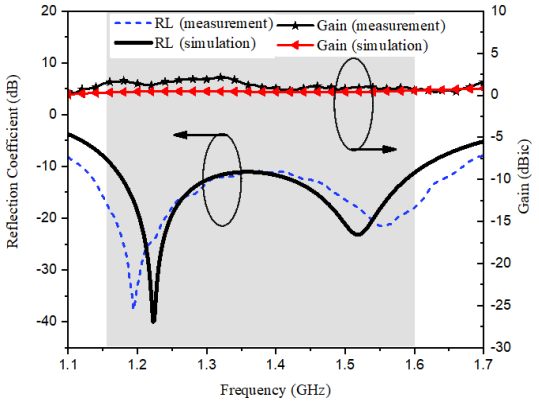

FIGURE 13. The simulated and measured for reflection coefficient and realized gain of the proposed antenna.

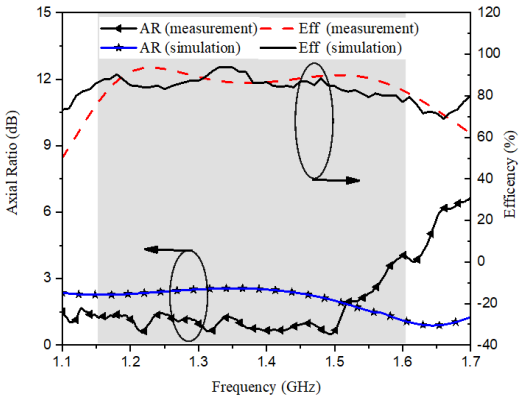

FIGURE 14. The simulated and measured axial ratio and efficiency of the proposed antenna.

Benha Electronics Company and measured in a Microwave and Antenna laboratory at the Faculty of Engineering in Ain Shams University using Agilent Vector Network Analyzer N9918A (VNA) and an anechoic chamber as shown in Fig. 12.

1) REFLECTION COEFFICIENT AND REALIZED GAIN

Fig. 13 shows the simulated and measured reflection coefficient and realized gain. The antenna covers the whole GNSS frequency band from 1.16 GHz to 1.61 GHz with a reflection coefficient better than -10 dB (VSWR $\leq$ 2) achieving an FIBW of 32.5%. The two resonant frequencies

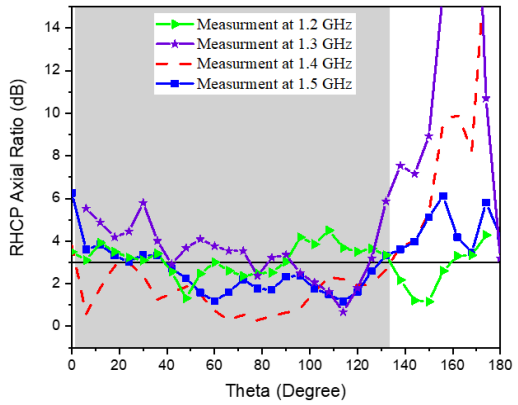

FIGURE 15. Measured the AR of the proposed antenna at various frequencies across the elevation angle.

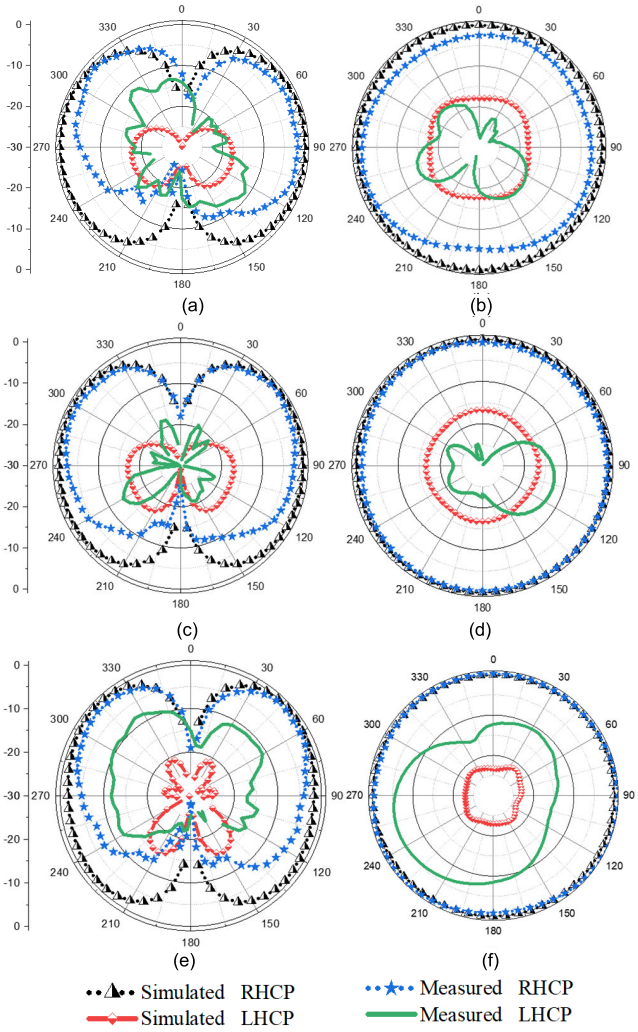

FIGURE 16. The simulated and measured radiation patterns: (a) XZ plane, 1.2 GHz; (b) XY plane, 1.2 GHz; (c) XZ plane, 1.4 GHz; (d) XY plane, 1.4 GHz; (e) XZ plane, 1.6 GHz; (f) XY plane, 1.6 GHz.

(LRF and URF) are slightly shifted due to fabrication tolerances. The antenna achieves a maximum gain of 2.1 dBic at the XY plane ($\theta = 90°$, $\phi =$ any).

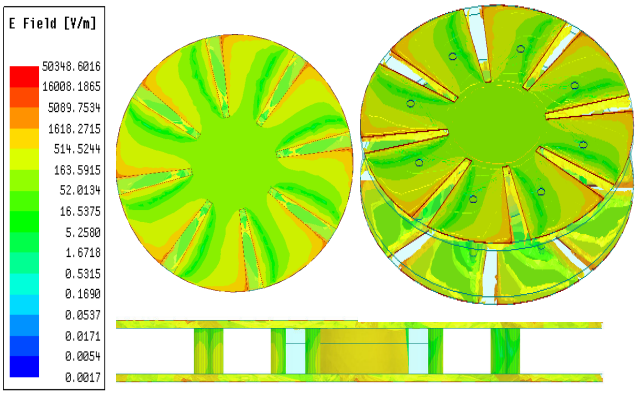

FIGURE 17. The simulated E-field distributions of the proposed antenna array at Pin = 1W.

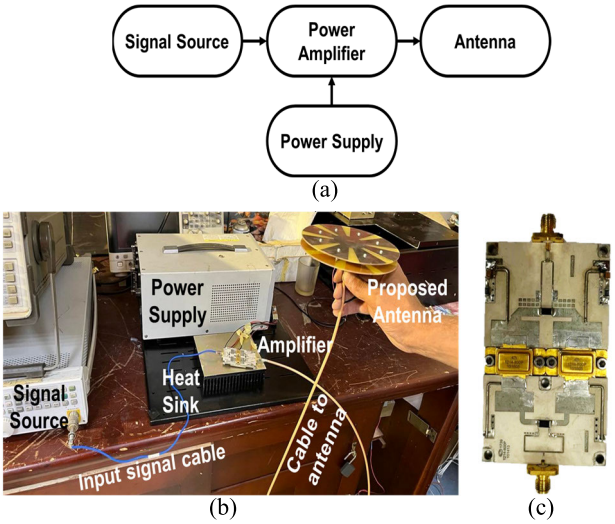

FIGURE 18. (a) The simple block diagram of the power handling test setup; (b) the overall test setup of the proposed antenna; (c) a Microsemi 1214-800p power amplifier module.

2) EFFICIENCY AND AXIAL RATIO

The total efficiency of the proposed antenna is shown in Fig. 14. Based on the measured realized gain and directivity, the antenna has an efficiency of 85±5% across the operating frequency band. The AR against frequency is measured at the X-axis and illustrated in Fig. 14. However, the AR is almost identical in the whole XY plane ($\theta = 90°$, $\phi =$ any) due to the symmetry of the antenna structure around the Z-axis. It is evident that the antenna offers a good AR below 3 dB throughout the operating frequency band. The simulated AR covers an FARBW of 42.8 % (from 1.1 to 1.7 GHz) while the measured AR covers an FARBW of 37.6% (from 1.1 to 1.61 GHz). This slight shrink in the FARBW may be due to the fabrication tolerances. However, the whole GNSS frequency band is covered with good CP radiation in both cases. The overlapped fractional bandwidth (FBW) between FIBW and FARBW is 32.5% (1.16 GHz to 1.61 GHz) which is broad enough to cover all GNSS bands.

TABLE 2. A comparison of the proposed antenna to CP omnidirectional antenna reported designs.

Ref	Centre Freq (GHz)	FIBW (%)	FARBW (%)	Overlapped FBW (%)	Max gain (dBic)	ARHPBW (°)	Dimensions (λ_0)
[2]	2.4	16.6	14.8	14.8	1.1	360° × 110°	0.376×0.376×0.028
[3] **	2.96	57.8	31	29.38	0.67	360° × 55°	0.41×0.41×0.1
[4]	2.4	19.8	25.2	19.8	2.5	360° × 50°	0.48×0.48×0.024
[5]	1.561	4.4	6.4	4.4	1.5	360° × 35°	0.24×0.24×0.12
[6]	2.5	30	30	30	0.5	360° × 110°	0.5×0.5×0.08
[7]	1.53	25.1	22.5	14.24	0.7	360° × 110°	0.402×0.402×0.082
[11]	2.41	16.8	4.9	4.9	-1.25	360° × 35°	0.68×0.68×0.048
[15]	1.2	66.7	57.7	53.4	0.9	360° × 10°	0.4×0.4×0.5
Proposed	**1.385**	**32.5**	**37.6**	**32.5**	**2.1**	**360° × 132°**	**0.34×0.34×0.05**

Bandwidth for −10dB S_{11} and 3dB AR.
*The proposed results have outperformed the underlined numbers.
**Measured results are not included. So, only simulated results are tabulated.

To guarantee an efficient CP performance over a wide spatial coverage (not only at the XY plane), the AR is measured over the elevation angle (θ) at various frequencies and presented in Fig.15. It is clear that the proposed antenna maintains its AR below 3 dB over a wide elevation angle of 132° (from 2° to 134°) at the central frequency (1.4 GHz).

3) RADIATION PATTERNS

Fig. 16 shows the normalized simulated and measured right-hand CP (RHCP) and left-hand CP (LHCP) radiation patterns in the XZ plane (V-plane) and XY plane (H-plane) respectively at 1.2 GHz, 1.4 GHz and 1.6 GHz. Due to the symmetry of the antenna structure, the proposed antenna radiates a stable omnidirectional CP radiation pattern throughout its operating frequency band. The antenna has a uniform 360° coverage in the H-plane and 8-shape patterns in the V-plane. The cross-polarization discrimination ratio (XPD) of the radiation patterns is better than 16.5 dB. XPD is defined as the ratio between the co-pol (RHCP) and cross-pol (LHCP) and is linked to the AR by [23]:

$$XPD\,(dB) = 20\log_{10}\left(\frac{AR+1}{AR-1}\right) \tag{3}$$

4) POWER HANDLING CAPABILITY

The maximum handling power is calculated according to the square relationship between power and electric field intensity as [24], [25]:

$$P_{max} = \left(\frac{E_{br}}{E_{max}}\right)^2 P_{in} \tag{4}$$

where:

P_{max}: the max power capacity
P_{in}: the input power
E_{br}: the electric field breakdown threshold (20 Mv/m for FR4-epoxy at L-band) [26]
E_{max}: the max electric field intensity when P_{in} is applied.

By applying a 1W input power at the excitation port through simulation, the maximum field intensity that appears across the whole structure is E_{max} = 50348.4 V/m as shown in Fig. 17. Therefore, P_{max}, theoretically, equals 157.7 kW which makes the proposed antenna an excellent candidate for a high-power GNSS anti-attacking system.

It is worth noting that this theoretical value is much far to be practically applied. So, to validate the performance of the proposed antenna at high input power, practically, a test setup has been set as shown in the block diagram in Fig. 18(a). A signal source has been adjusted to generate a signal at a frequency within the frequency band of the proposed antenna. Then, the generated signal is fed to a high-power amplifier which is biased using a DC power supply. The amplified high-power signal is, subsequently, fed to the proposed antenna.

The test setup has been implemented using a pulsed signal source that generates a signal at 1.3 GHz with a 10% duty cycle. All the cables have been considered during the calibration phases before the measurements. A Microsemi 1214-800p power amplifier module (which gives an 800w peak output power) has been used to amplify the pulsed signal. This setup gives the highest output power available in our lab at that frequency band. The 800w-pulsed signal is fed to the proposed antenna. The whole setup is presented in Fig. 18(b) while the amplifier module is shown in Fig. 18(c). The overall system has run for a few minutes without any notable failure or degradation in performance and no change in all the previous results of the antenna.

IV. COMPARISON

To justify the performance of the proposed antenna, a comparison to reported designs of omnidirectional CP antennas, based on measured results, is tabulated in TABLE 2. It is obvious that the proposed antenna outperforms all the other reported designs in terms of the overlapped FBW. The proposed antenna also has a relatively high realized gain and a relatively small size. Moreover, the proposed antenna offers the widest axial ratio half-power beamwidth (ARHPBW) which demonstrates the largest CP spatial coverage. These features in addition to its high PHC make the proposed antenna suitable to be used as a CP radiator in a GNSS anti-attacking system.

V. CONCLUSION

The antenna, which incorporates a circular disc with centre feeding, is optimized for performance. A design approach for a novel omnidirectional circular polarized antenna is proposed, studied to cover the whole GNSS frequency band (1.16–1.61) GHz and validated by fabricating a prototype as well as measuring its parameters. The proposed design offers an omnidirectional pattern with a maximum gain of 2.1 dBic and a low profile suitable to be implemented in portable systems that prevent the attacks of GNSS-guided vehicles. Moreover, the LRF shifts up and merges with the URF to realize a broad bandwidth with two resonances to cover almost the whole GNSS frequency band. The antenna bandwidth can be improved at the cost of the antenna size by increasing its height. However, if we take the application of the proposed antenna into account, the achieved bandwidth is sufficient to cover the whole GNSS system. Therefore, there is no need to increase the antenna size for out-of-band signal coverage. The antenna can handle a high power of up to 157.7 kW while maintaining CP radiation over a wide span of angles (132° in elevation and 360° in azimuth). Thus, the proposed antenna is a good candidate for an anti-attack system against UAVs guided by GNSS to safeguard vital targets.

REFERENCES

[1] D. Borio and C. Gioia, "GNSS interference mitigation: A measurement and position domain assessment," *Navigat., J. Inst. Navigat.*, vol. 68, no. 1, pp. 93–114, Mar. 2021.

[2] Y. Shi and J. Liu, "Wideband and low-profile omnidirectional circularly polarized antenna with slits and shorting-vias," *IEEE Antennas Wireless Propag. Lett.*, vol. 15, pp. 686–689, 2016.

[3] Y. Xiang and Z.-H. Ma, "Design of a compact wideband omnidirectional circularly polarized antenna," in *Proc. Cross Strait Radio Sci. Wireless Technol. Conf. (CSRSWTC)*, Dec. 2020, pp. 1–3.

[4] Y.-M. Cai, S. Gao, Y. Yin, W. Li, and Q. Luo, "Compact-size low-profile wideband circularly polarized omnidirectional patch antenna with reconfigurable polarizations," *IEEE Trans. Antenna Propag.*, vol. 64, no. 5, pp. 2016–2021, May 2016.

[5] C.-Y. Liu and Q.-X. Chu, "A compact omnidirectional circularly polarized antenna," in *Proc. 12th Eur. Conf. Antennas Propag. (EuCAP)*, 2018, pp. 1–2.

[6] H. H. Tran, N. Nguyen-Trong, and H. C. Park, "A compact wideband omnidirectional circularly polarized antenna using TM_{01} mode with capacitive feeding," *IEEE Antennas Wireless Propag. Lett.*, vol. 18, no. 1, pp. 19–23, Jan. 2019.

[7] L. Peng, B. Wang, B. Wang, X. Jiang, S. Li, and C. Ruan, "Bandwidth enhancement of the omni-directional and circularly-polarized EZR-MZR antenna," *Int. J. RF Microw. Comput.-Aided Eng.*, vol. 31, no. 8, Aug. 2021, Art. no. e22731, doi: 10.1002/mmce.22731.

[8] A. Chandra, N. Mishra, R. Kumar, K. Kumar, and H. Y. Patil, "A superstrate and FSS embedded dual band waveguide aperture array with improved far-field characteristics," *Microw. Opt. Technol. Lett.*, vol. 65, no. 1, pp. 341–347, Jan. 2023.

[9] H. Shi, J. Li, J. Shi, J. Chen, Z. Li, S. Zhu, T. A. Khan, and A. Zhang, "Miniaturized circularly polarized patch antenna using coupled shorting strip and capacitive probe feed," *AEU, Int. J. Electron. Commun.*, vol. 98, pp. 235–240, Jan. 2019.

[10] R. Kumar, S. R. Thummaluru, and R. K. Chaudhary, "Improvements in Wi-MAX reception: A new dual-mode wideband circularly polarized dielectric resonator antenna," *IEEE Antennas Propag. Mag.*, vol. 61, no. 1, pp. 41–49, Feb. 2019.

[11] Y. Ning, Y. Fan, and Y. Dong, "Omnidirectional circularly polarized antenna based on dual zeroth-order resonances," in *Proc. IEEE Asia–Pacific Microw. Conf. (APMC)*, Dec. 2019, pp. 816–818.

[12] H. Nawaz, X. Liang, M. S. Sadiq, J. Geng, and R. Jin, "Circularly-polarized shaped pattern planar antenna for aerial platforms," *IEEE Access*, vol. 8, pp. 7466–7472, 2020.

[13] J. Li, Y. Huang, and G. Wen, "Design of a compact tri-band omni-directional circularly polarized antenna," in *Proc. IEEE Int. Symp. Antennas Propag. USNC/URSI Nat. Radio Sci. Meeting*, Jul. 2018, pp. 121–122.

[14] A. Kumar, A. A. Althuwayb, D. Chaturvedi, R. Kumar, and F. Ahmadfard, "Compact planar magneto-electric dipole-like circularly polarized antenna," *IET Commun.*, vol. 16, no. 20, pp. 2448–2453, 2022.

[15] X. Cai and K. Sarabandi, "Broadband omnidirectional circularly polarized antenna with asymmetric power divider," *IEEE Trans. Antennas Propag.*, vol. 68, no. 7, pp. 5171–5181, Jul. 2020.

[16] S. R. Peng, C. W. Yuan, and T. Shu, "Analysis of a high power microwave radial line slot antenna," *Rev. Sci. Instrum.*, vol. 84, no. 7, pp. 074701-1–074701-7, Jul. 2013.

[17] X.-Q. Li, Q.-X. Liu, X.-J. Wu, L. Zhao, J.-Q. Zhang, and Z.-Q. Zhang, "A GW level high-power radial line helical array antenna," *IEEE Trans. Antennas Propag.*, vol. 56, no. 9, pp. 2943–2948, Sep. 2008.

[18] X. Ma, F. Yang, P. Yang, R. Wang, Y. Yan, and K. Chen, "Design of a novel compact slotted cavity with shaped beam for high power microwave feed antenna using asymmetric high order mode," *IEEE Access*, vol. 7, pp. 101459–101470, 2019.

[19] H. Zhang, R. Meng, Z. Xia, and Q. Zhu, "A novel substrate integrated waveguide slot antenna with high power-handling capacity," in *Proc. IEEE Antennas Propag. Soc. Int. Symp. (APSURSI)*, Jul. 2014, pp. 1037–1038.

[20] G.-X. Kong, X.-Q. Li, S.-C. Ni, J.-Q. Zhang, and Q.-F. Wang, "Design of dual-band elliptical patch reflectarray antenna with high power handling capacity," in *IEEE MTT-S Int. Microw. Symp. Dig.*, Sep. 2020, pp. 1–3.

[21] G.-X. Kong, X.-Q. Li, S.-C. Ni, J.-Q. Zhang, and Q.-F. Wang, "Design of a millimeter wave helical reflectarray antenna with high power handling capacity," in *Proc. Int. Symp. Electron. Inf. Technol. Commun. Eng.*, vol. 1607, Jun. 2020, Art. no. 012007.

[22] J. S. Subirana, J. M. J. Zornoza, and M. Hernández-Pajares, *GNSS Data Processing: Fundamentals and Algorithms*. Paris, France: ESA, May 2013.

[23] R. Galuscak, P. Hazdra, and M. Mazanek, "Compact circular/linear polarization dual-band prime-focus feed for space communication," *Int. J. Antennas Propag.*, 2012, doi: 10.1155/2012/860951.

[24] R. Meng, Y. Xia, Y. Guo, and Q. Zhu, "An *X*-band 48-way leaky waveguide antenna with high aperture efficiency and high-power capacity," *IEEE Trans. Antennas Propag.*, vol. 66, no. 12, pp. 6799–6809, Dec. 2018.

[25] A. M. Eid, A. Alieldin, A. M. El-Akhdar, A. F. El-Agamy, W. M. Saad, and A. A. Salama, "A novel high power frequency beam-steering antenna array for long-range wireless power transfer," *Alexandria Eng. J.*, vol. 60, no. 2, pp. 2707–2714, Apr. 2021.

[26] S. J. Mumby and J. Yuan, "Dielectric properties of FR-4 laminates as a function of thickness and the electrical frequency of the measurement," *J. Electron. Mater.*, vol. 18, no. 2, pp. 287–292, Mar. 1989, doi: 10.1007/BF02657420.

MOHAMED AKMAL received the B.S. degree in electronics and communications engineering from Alexandria University, Alexandria, Egypt, in 2015. He is currently pursuing the M.S. degree in electronics and communications engineering with Ain Shams University, Cairo, Egypt. He is currently a Lecturer with the Egyptian Air Defence College.

AHMED ALIELDIN (Member, IEEE) received the B.Sc. degree in radar engineering from the Military Technical College, Egypt, in 2005, the M.Sc. (Eng.) degree in antenna and microwave propagation from Alexandria University, Egypt, in 2013, and the Ph.D. degree in antennas and electromagnetics from the University of Liverpool, U.K., in 2019. His academic research activities and Ph.D. were centered on antenna designing and measurements with an emphasis on mobile communication applications. In addition to working in academia, he also held various positions throughout more than 15 years of working in the industry. He has authored/coauthored many articles in leading international journals and conference proceedings. He has filed a patent. His academic research interests include novel textile antennas, multiple-input multiple-output antennas, base station antennas, satellite antennas, transparent antennas, and phased-MIMO radar antennas. He serves as a technical reviewer for leading academic journals and conferences and served as the session chair for many international conferences.

ANGIE R. ELDAMAK (Member, IEEE) was born in Damietta, Egypt, in 1980. She received the B.Sc. and M.Sc. degrees in electrical engineering from Ain Shams University, Cairo, Egypt, in 2002 and 2006, respectively, and the Ph.D. degree in electrical engineering from Ryerson University, Toronto, Canada, in 2013. Since November 2014, she has been with the Electronics and Communications Engineering Department, Ain Shams University, where she is currently an Associate Professor. She has 15 years of microwave research and development experience, specifically in designing passive antenna systems as well as fabrication and testing for biosensing and wireless communications applications, and eight years of research and development experience in designing, implementing, and modeling fiber-based systems. Her current research interests include antennas, microwave-based sensors, and passive microwave components.